water

MDPI

Article

Adsorption Studies on Magnetic Nanoparticles Functionalized with Silver to Remove Nitrates from Waters

Yesica Vicente-Martínez [1], Manuel Caravaca [1,*], Antonio Soto-Meca [1], Miguel Ángel Martín-Pereira [1] and María del Carmen García-Onsurbe [2]

[1] Department of Science, University Centre of Defence at the Spanish Air Force Academy, Ministry of Defence-Technical University of Cartagena, C/Coronel López Peña s/n, Santiago de la Ribera, 30720 Murcia, Spain; yesica.vicente@cud.upct.es (Y.V.-M.); antonio.soto@cud.upct.es (A.S.-M.); mmarpe5@mde.es (M.Á.M.-P.)

[2] Campus Alfonso XIII, Technical University of Cartagena, 30203 Cartagena, Spain; mariadelcarmen.garcia2@edu.upct.es

* Correspondence: manuel.caravaca@cud.upct.es

Abstract: This paper presents a novel procedure for the treatment of contaminated water with high concentrations of nitrates, which are considered as one of the main causes of the eutrophication phenomena. For this purpose, magnetic nanoparticles functionalized with silver (Fe_3O_4@AgNPs) were synthesized and used as an adsorbent of nitrates. Experimental conditions, including the pH, adsorbent and adsorbate dose, temperature and contact time, were analyzed to obtain the highest adsorption efficiency for different concentration of nitrates in water. A maximum removal efficiency of 100% was reached for 2, 5, 10 and 50 mg/L of nitrate at pH = 5, room temperature, and 50, 100, 250 and 500 µL of Fe_3O_4@AgNPs, respectively. The characterization of the adsorbent, before and after adsorption, was performed by energy dispersive X-ray spectroscopy, scanning electron microscopy, Brunauer-Emmett-Teller analysis and Fourier-transform infrared spectroscopy. Nitrates can be desorbed, and the adsorbent can be reused using 500 µL of NaOH solution 0.01 M, remaining unchanged for the first three cycles, and exhibiting 90% adsorption efficiency after three regenerations. A deep study on equilibrium isotherms reveals a pH-dependent behavior, characterized by Langmuir and Freundlich models at pH = 5 and pH = 1, respectively. Thermodynamic studies were consistent with physicochemical adsorption for all experiments but showed a change from endothermic to exothermic behavior as the temperature increases. Interference studies of other ions commonly present in water were carried out, enabling this procedure as very selective for nitrate ions. In addition, the method was applied to real samples of seawater, showing its ability to eliminate the total nitrate content in eutrophized waters.

Keywords: adsorption; magnetic nanoparticles; nitrate; pollutant removal; water remediation

Citation: Vicente-Martínez, Y.; Caravaca, M.; Soto-Meca, A.; Martín-Pereira, M.Á.; García-Onsurbe, M.d.C. Adsorption Studies on Magnetic Nanoparticles Functionalized with Silver to Remove Nitrates from Waters. *Water* **2021**, *13*, 1757. https://doi.org/10.3390/w13131757

Academic Editor: Zhenli He

Received: 22 May 2021
Accepted: 22 June 2021
Published: 25 June 2021

1. Introduction

Industrial and agricultural activities have resulted in an increase of the concentration of nutrients in water. Among them, nitrates are considered as one of the most diffused contaminant, especially because of their high solubility in water and low retention by soil particles [1]. Eutrophication is the most important process of water pollution in aquatic environments such as lakes, rafts, rivers or reservoirs [2]. This process is caused by the excess of nutrients in water, mainly nitrogen and phosphorus, mostly arising from human activity. Moreover, eutrophication affects the quality of waters since they acquire a foul smell as rot increases and the oxygen depletes. The smell of these waters can lead to economic losses (tourism, areas that lose value, among others), respiratory problems and their consumption can cause health problems in the nearby areas [3–5].

For these reasons, nowadays, many methods to remove nitrates from water samples have been developed. Among them, procedures based on catalysis [1,6–9], electrocoagulation [10–12] and photocatalysis [13,14] are common.

Approaches for removing nitrates based on biological treatments were also widely used some years ago [1,15–18]. However, these techniques have been superseded by other methods that lead to better results in terms of removal efficiency, quickness and simplicity. In this sense, methods for removing nitrates based on adsorption lead to high removal efficiencies. Different materials have been used as nitrate adsorbents, such as carbon activated and zeolite [19], amberlite [20], several resines [21,22], composites [23] and microalgae [24]. Notwithstanding, these procedures do not achieve the total removal of nitrates in water compared to the work presented in this article.

The use of nanoparticles to remove nitrates in water samples has been studied in recent years, obtaining good results in relation to removal efficiency. However, these procedures are not very fast or easy to carry out, in general [25–29]. By comparison with our approach, these methods involve more tedious experimental processes with higher costs, higher temperatures, or longer times to achieve the maximum adsorption of nitrates, which in no case reaches 100% of the removal of the pollutant. The procedure presented in this work represents a great advance in the elimination of nitrates in water over the aforementioned, presenting numerous advantages such as the total adsorption of high concentrations of nitrates in water in just a few seconds, under mild experimental conditions and using a very low adsorbent dose.

Consequently, in this study we present a novel, very simple and fast method for adsorption of nitrates from aqueous samples using magnetic core functionalized with silver nanoparticles (Fe_3O_4@AgNPs) as an adsorbent. The choice of Fe_3O_4@AgNPs is primarily based on the quick and easy removal of magnetic nanoparticles from aquatic environments using a magnet, as shown in recent literature [30–32]. Moreover, a novel study showed the notable increase in the adsorption efficiency to eliminate phosphates in water when the adsorbent was functionalized with silver nanoparticles [33]. Phosphates and nitrates present similar characteristics, so the effect of silver on nitrate adsorption resulted positive, in the same way. However, to the best of our knowledge, Fe_3O_4@AgNPs was not previously used as an adsorbent for nitrate removal. Experimental conditions such as pH, temperature, contact time and adsorbent dose have been studied to achieve maximum nitrate removal efficiency. After the adsorption process, Fe_3O_4@AgNPs can be recycled and reused. Interference studies were carried out, providing this process as very selective for nitrate ions in the presence of other ions commonly present in water.

2. Materials and Methods

2.1. Materials

For all the experiments conducted, the solvents and reagents employed were of analytical reagent grade. Pure water obtained with a Millipore system (Millipore, Bedford, MA, USA) was used exclusively. All the solutions were stored in polypropylene or polytetrafluoroethylene vessels. Nitrate solutions were prepared with sodium nitrate purchased from Sigma Aldrich. Nanoparticles were prepared using $FeCl_3 \cdot 6H_2O$, $FeCl_2 \cdot 4H_2O$ and concentrated ammonia solution from Sigma Aldrich. Nitric acid and potassium iodide were purchased from Panreac.

Permanent Nd-Fe-B magnets from Supermagnete, agitator system model AM20-D from Argolab and ultrasound bath model 4820 from PCE instruments were used to prepare the nanoparticles and conduct the experiments. Nitrate concentrations were determined using UV-Vis Nanodrop Spectrophotometer model 2000 (Thermo Fisher Scientific, Madrid, Spain) operating at 220 nm.

2.2. Preparation of Fe_3O_4@AgNPs

Water solution (20 mL) was heated at 80 °C and steadily under nitrogen atmosphere. Afterwards, 0.56 g $FeCl_3 \cdot 6H_2O$, 0.2 g $FeCl_2 \cdot 4H_2O$ and 2 mL of concentrated ammonia

solution were added. The mixture was stirred for 10 min. Using a permanent magnet, the particles were separated, and the supernatant solution was rejected. A brown solid was obtained (Fe_3O_4), washed three times with water and suspended in 20 mL of water. Then, a solution of silver nitrate at concentration of 0.011 g L^{-1} (5.7 mL) were added and mixture was stirred for 5 min. After that, the nanoparticles obtained (Fe_3O_4@AgNPs) were washed several times with water using and suspended in 20 mL of water.

Iron oxide-based magnetic nanoparticles are recognized to be good as adsorbents, but magnetic and long-range electrostatic interactions make them aggregate [34]. Their synthesis by modifying the surface with nanoparticles avoids this fact and enhances adsorption efficiency by incorporating new active sites [35,36], thus giving Ag NPs a leading role.

2.3. Nitrates Adsorption Procedure

The adsorption procedure has been studied for different concentrations of nitrates in waters, C_e. Specifically, adsorption is carried out using 10 mL of aqueous samples placed in polypropylene tubes at nitrate concentrations of 2, 5, 10 and 50 mg L^{-1}. 200 µL of acetate buffer solution (0.1 M, pH = 5) were added. Then 100, 100, 250 and 500 µL of Fe_3O_4@AgNPs were incorporated to the mixtures for the respective solutions at different nitrate concentration (2, 5, 10 and 50 mg L^{-1}). After shaking at 60 s, the adsorbent was separated by placing the magnet at the bottom of the tube. The supernatant was analyzed by spectrophotometry, showing the total nitrate removal in every solution.

The adsorption capacity of the nitrate adsorbent, known as q_e (mg g^{-1}), was calculated according to the following equation:

$$q_e = \frac{(C_0 - C_t)V}{m} \quad (1)$$

where C_0 (mg L^{-1}) and C_t (mg L^{-1}) are the of nitrate concentrations in aqueous solution at the initial and after removing process. V (L) is the volume of the solution and m (mg) is the mass of the Fe_3O_4@AgNPs.

3. Results and Discussion

3.1. Characterization of Fe_3O_4@AgNPs

In order to check the nitrate adsorption onto the adsorbent surface, Fe_3O_4@AgNPs was characterized before and after adsorption process. Figure 1a shows a scanning electron microscopy (SEM) image of Fe_3O_4@AgNPs, where the well-differentiated lighter structures correspond to Ag on the Fe_3O_4 surface, due to its higher atomic number. The corresponding mapping SEM image also reveals the presence of Ag on the adsorbent, highlighted in blue color and labeled in the plot (Figure 1b).

To confirm the presence of Ag in the adsorbent, Figure 2 shows the energy dispersive X-ray spectroscopy (EDX) pattern for Fe_3O_4@AgNPs associated to the SEM, where the characteristic signal for Ag at 2.984 keV is shown. Additionally, strong characteristic signals for Fe, at 0.705 and 6.398 keV, and for O, at 0.525 keV, indicate the presence of Fe_3O_4.

Figure 3 shows Fourier-transform infrared spectroscopy (FTIR) spectrum for the adsorbent after the adsorption process in order to confirm the presence of nitrate. The characteristic nitrate signals are marked. The vibrational peak for N=O stretching appears at 1600 cm^{-1}, the NO_3 asymmetric stretching is shown at 1380 cm^{-1}, while the NO_3 symmetric stretching peak is observed at 800 cm^{-1}, as supported by the literature [37].

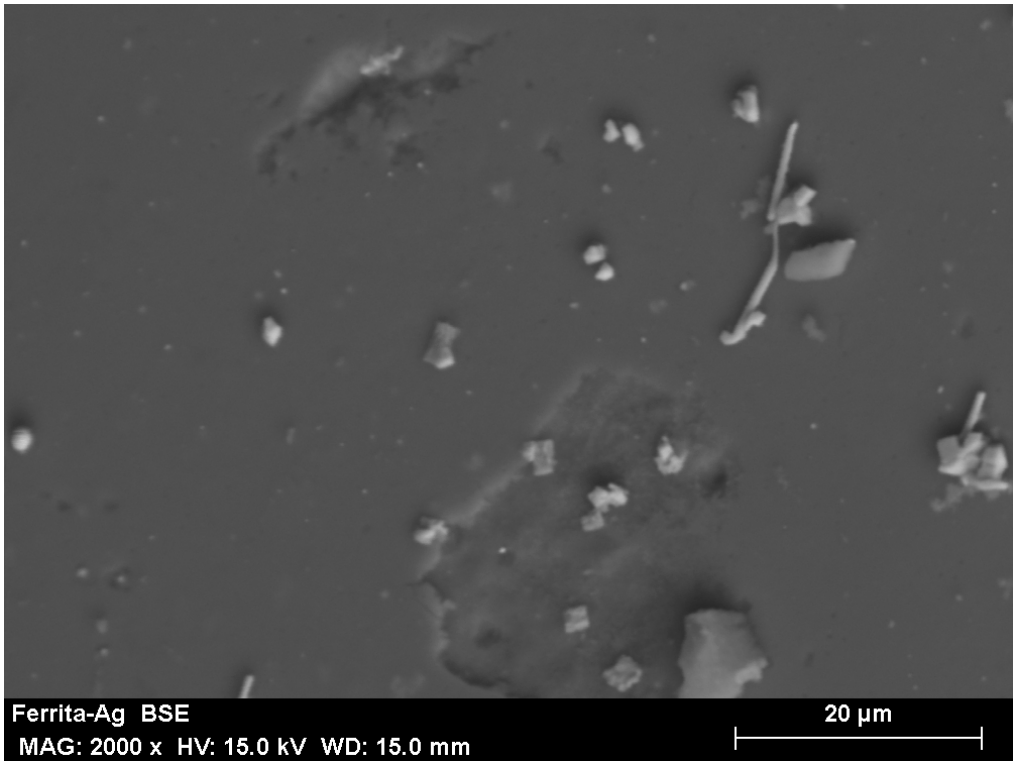

(**a**)

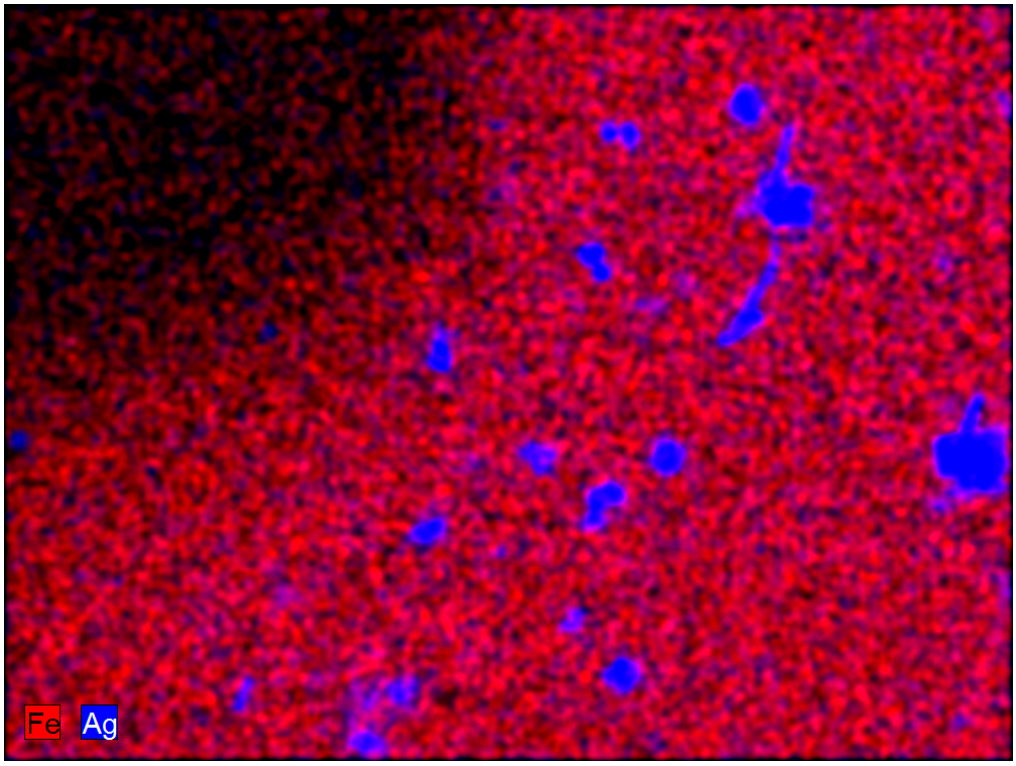

(**b**)

Figure 1. SEM image (**a**) and its corresponding mapping (**b**) for Fe_3O_4@AgNPs. The presence of Ag in the sample is revealed through the lighter structures (**a**) and the highlight in blue color (**b**).

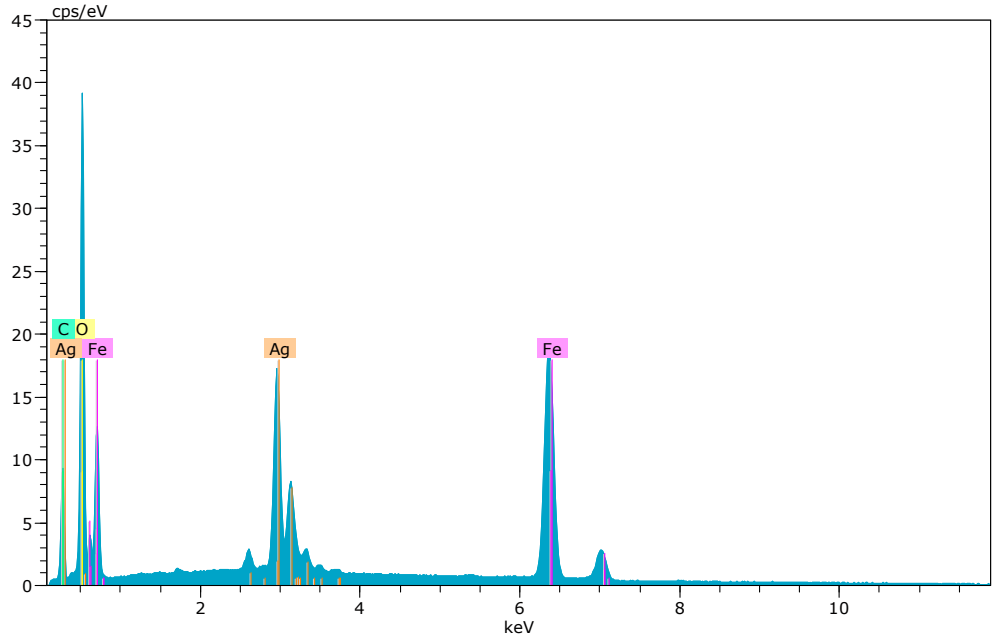

Figure 2. EDX pattern for Fe_3O_4@Ag adsorbent. Characteristic peaks for Ag (2.984 keV), Fe (0.705 and 6.398 keV), and O (0.525 keV) are shown in the figure.

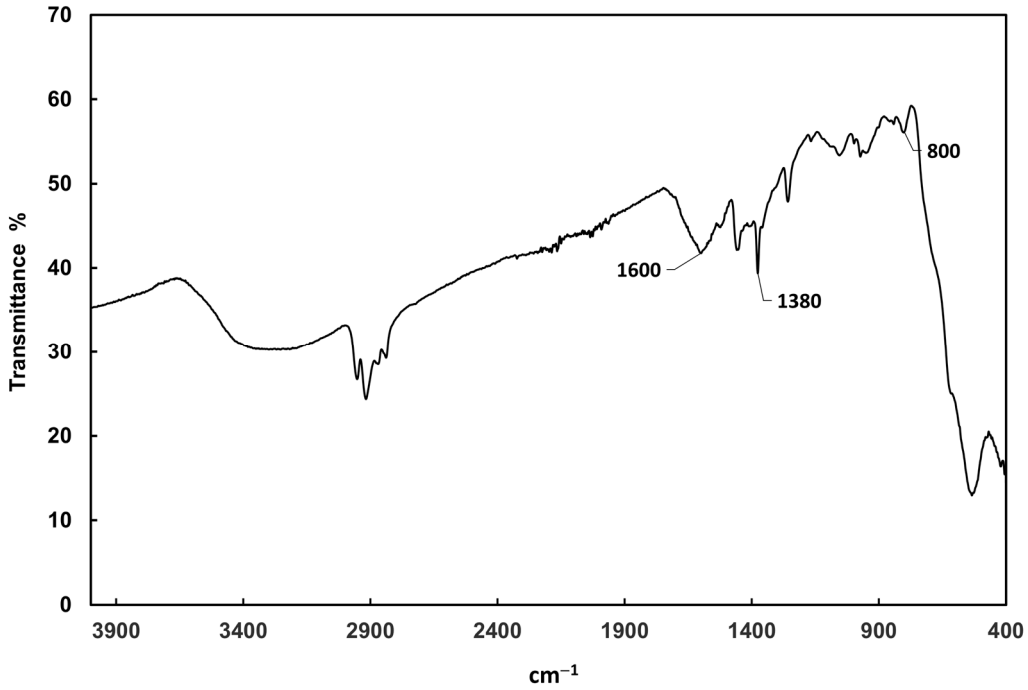

Figure 3. FTIR spectrum for Fe_3O_4@Ag after nitrate adsorption. Signals at 800, 1380 and 1600 cm^{-1} correspond to NO_3 symmetric stretching peak, NO_3 asymmetric stretching peak and vibrational peak for N=O stretching, respectively.

Complementary, Figure 4 shows a SEM image after the adsorption process, where the darker structures are associated to nitrates, due to the lower atomic number of N. Additionally, the spectrophotometry performed before the adsorption detects signal at 220 nm, which is indicative of the presence of nitrates in the aqueous sample. After the removal of the magnetic nanoparticles with the magnet the signal is zero, revealing that the nitrates were adsorbed onto the Fe_3O_4@AgNPs.

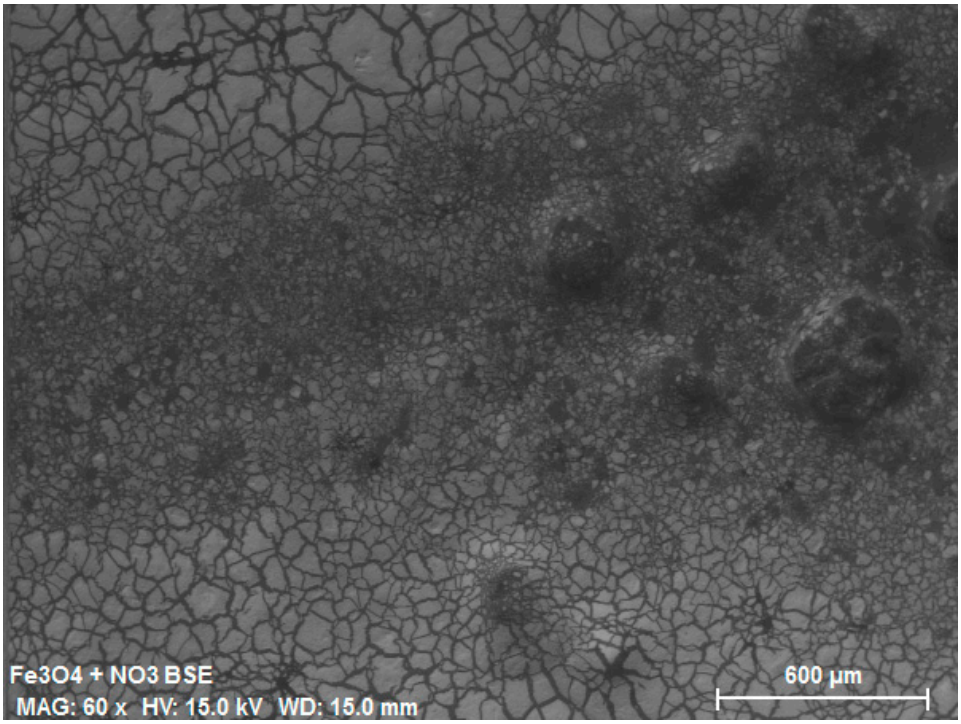

Figure 4. SEM image for Fe_3O_4@AgNPs after the adsorption. Darker structures are associated to the presence of nitrates, due to the lower atomic number of N.

A Brunauer-Emmett-Teller test determined the contact surface area of Fe_3O_4@AgNPs, equal to 116.476 m^2/g. One of the roles of Ag NPs is to increase the specific surface area of adsorption, as it was demonstrated by previous studies by the authors [33].

3.2. Effect of pH on Nitrate Removal by Fe_3O_4@AgNPs

The effect of pH on the adsorption of nitrates was investigated by determining the adsorption efficiency within the range [1–9], employing nitrate concentrations equal to 2, 5, 10 and 50 mg L^{-1}. The results are shown in Figure 5, which indicates that there is a common pH range, 4–5, presenting the highest adsorption efficiency for all concentrations. The error bars are smaller than the size of the symbols in Figure 5 and the following, not shown.

The point of zero charge (PZC) of the aqueous system is considered as one of the main parameters that affects the behavior of the adsorbents [38]. In general, the influence of pH on anion exchange reaction is principally due to the effect of competitive hydroxyl ions and anions [39]. The PZC of adsorbent Fe_3O_4@Ag is found to lie within the range [6.03–6.7] [40]. For values pH > PZC, the surface of Fe_3O_4@Ag becomes negatively charged and there is a repulsion force between the adsorbent and the nitrate anion, so the adsorption capacity decreases. For values pH < PZC, the surface of the adsorbent becomes positively charged, which results in the electrostatic attraction between the nitrate anion and the surface, and so the adsorption efficiency increases. Nevertheless, at very low pH, the electrostatic attraction is drastically reduced due to the ionic strength, which measures the effect of ions in solution on the electrostatic potential [41]. An increase in the ionic strength of the solution lowers the electrostatic interactions, either attractive or repulsive, due to a screening effect of the surface charge caused by the reduction of pH [42], thus shielding electrostatic interactions. For all plots in Figure 5, this effect is regarded from pH < 4, being the screening reduced as the nitrate concentration decreases, in concordance with recent surface-force measurements showing that the typical screening length increases with ion concentration [43].

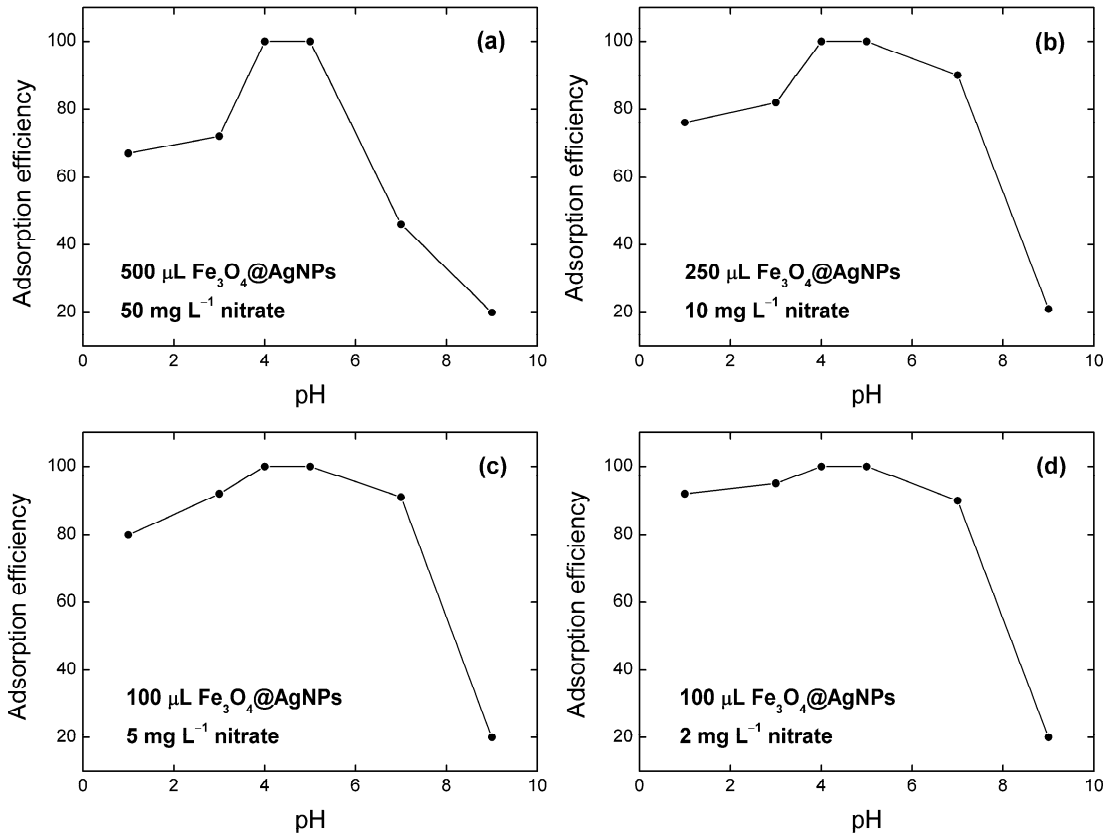

Figure 5. Dependence of the adsorption efficiency on pH for different volumes of Fe_3O_4@AgNPs and nitrate concentrations, respectively: (**a**) 500 μL and 50 mg L^{-1}, (**b**) 250 μL and 10 mg L^{-1}, (**c**) 100 μL and 5 mg L^{-1}, (**d**) 100 μL and 20 mg L^{-1}. Screening of electrostatic interactions becomes greater as nitrate concentration increases.

The results in Figure 5 suggest that our procedure is especially suitable for treatment plants, where the pH and other factors can be regulated for water treatment. Nevertheless, application to waters in natural ecosystems such as seawater, which pH has a neutral-basic character [44], also provides a high adsorption efficiency, around 75% for pH between 7 and 8, as depicted from Figure 5b–d. These efficiencies are still high compared to the traditional methods usually employed [1,6,10]. For higher nitrate concentrations, such as that shown Figure 5a, water could be processed in treatment plants.

The adsorption mechanism can be regarded as a physicochemical adsorption. Semi-empirical quantum-chemical studies reveal that orbitals 5s and 5d of Ag could be responsible for the chemisorption of nitrate [45]. A physicochemical process agrees with thermodynamic studies presented in Section 3.7.

3.3. Effect of Adsorbent Dose and Performance Metrics

The effect of Fe_3O_4@AgNPs volume was studied in order to achieve the maximum nitrate efficiency removal in aqueous solutions, for nitrate concentrations equal to 2, 5, 10 and 50 mg L^{-1}. Volumes under study lied in the range (50, 750) μL. All experiments employed pH = 5 and 60 s of contact time between solution and adsorbent. Figure 6 shows that the maximum adsorption efficiencies for 2 (magenta empty inverted triangles), 5 (blue triangles), 10 (red dots) and 50 (black squares) mg L^{-1} nitrate concentrations were achieved by using 100, 100, 250 and 500 μL of adsorbent, respectively.

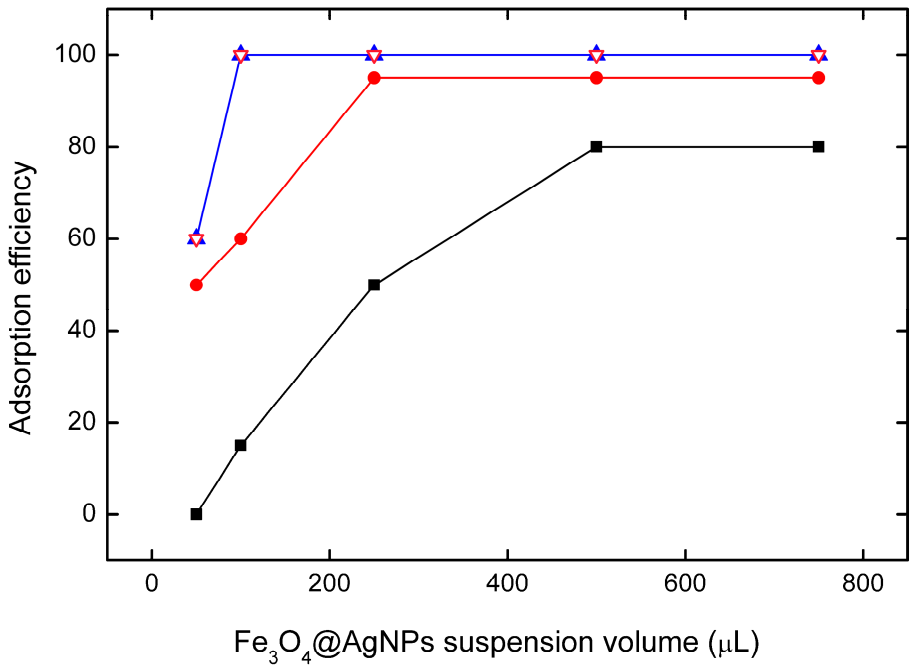

Figure 6. Dependence of the adsorption efficiency on the adsorbent (Fe_3O_4@AgNPs) suspension volume for nitrate concentrations equal to 50 mg L^{-1} (black squares), 10 mg L^{-1} (red dots), 5 mg L^{-1} (blue triangles) and 2 mg L^{-1} (magenta empty inverted triangles).

The variable q_e was calculated for each nitrate concentration versus the suspension volume of Fe_3O_4@AgNPs, increasing with the nitrate concentration. For this reason, to evaluate the adsorbent performances by reducing the bias it is appropriate to use the partition coefficient (*PC*) (mg g^{-1} μM^{-1}) [33,46], defined as:

$$PC = \frac{q_e}{\frac{C_0}{M}(1 - MRE)} = \frac{q_e}{\frac{C_f}{M}} \quad (2)$$

where C_0 the initial concentration of pollutant in the liquid sample (mg L^{-1}), C_f the final concentration of the liquid sample, M the molar mass (mg mM^{-1}) and *MRE* is the maximum removal efficiency. As depicted from Table 1, the *PC* diverges when *MRE* is 100%, and decreases as the *MRE* does.

Table 1. Performance metrics of Fe_3O_4@AgNPs employed for adsorption of different concentrations of nitrate species in water.

Optimum Conditions (Temperature (°C), pH)	Initial Nitrate Concentration (mg L^{-1})	Fe_3O_4@AgNPs Mass (mg)	Maximum Removal Efficiency (%)	Adsorption Capacity (mg g^{-1})	Partition Coefficient (mg g^{-1} μM^{-1})
25, 5	2	9.5	100	2.11	-
25, 5	2	7	100	2.86	-
25, 5	2	3.5	100	5.71	-
25, 5	2	1.4	100	14.29	-
25, 5	2	0.7	60	28.57	2214.29
25, 5	5	9.5	100	5.26	-
25, 5	5	7	100	4.17	-
25, 5	5	3.5	100	14.29	-
25, 5	5	1.4	100	35.71	-

Table 1. *Cont.*

Optimum Conditions (Temperature (°C), pH)	Initial Nitrate Concentration (mg L^{-1})	Fe_3O_4@AgNPs Mass (mg)	Maximum Removal Efficiency (%)	Adsorption Capacity (mg g^{-1})	Partition Coefficient (mg g^{-1} μM^{-1})
25, 5	5	0.7	60	71.43	163.16
25, 5	10	9.5	100	10.53	-
25, 5	10	7	100	14.29	-
25, 5	10	3.5	100	28.57	-
25, 5	10	1.4	95	71.43	8857.14
25, 5	10	0.7	95	142.86	17,714.29
25, 5	50	9.5	99	26.32	3263.16
25, 5	50	7	99	35.71	4428.57
25, 5	50	3.5	86	71.43	632.65
25, 5	50	1.4	80	157.57	1107.14
25, 5	50	0.7	80	357.14	2214.29

Table 1 shows that the *PC* diverges when MRE is 100% which occurs for every nitrate concentration in equilibrium situation. At fixed nitrate concentration, q_e increases as Fe_3O_4@AgNPs mass decreases. At fixed Fe_3O_4@AgNPs mass, q_e increases as nitrate concentration does.

3.4. Contact Time Effect

Kinetics of Langmuir-like physicochemical reversible processes are well described employing an efficient kinetic three-parameter model connecting both the equilibrium and kinetic viewpoints [33]:

$$Adsorption\ efficiency = (\alpha - \beta)\frac{(\beta/\alpha)e^{(\beta-\alpha)\gamma t}}{(\beta/\alpha)e^{(\beta-\alpha)\gamma t} - 1} + \beta \quad (3)$$

where t is the contact time for the adsorption process and α, β, γ are characteristic parameters. This model characterizes Langmuir-type adsorption processes matching kinetics and isotherms, unlike other models like the pseudo-first or pseudo-second order [47]. The time of contact between the adsorbent Fe_3O_4@AgNP and the solutions containing nitrate at different concentrations, 2, 5, 10 and 50 mg L^{-1}, was studied for pH = 5 (characterized by Langmuir isotherm, see Section 3.6) and adsorbent volumes equal to 50, 100, 250 and 500 µL, respectively. Contact times needed for achieving the maximum removal efficiency were 15, 30, 45 and 60 s for 2, 5, 10 and 50 mg L^{-1} nitrate concentrations, respectively. Figure 7 shows the dependence of the adsorption efficiency on the contact time for concentrations 50 mg L^{-1} (black dots) and 10 mg L^{-1} (red triangles). The solid lines represent the fits to the theoretical kinetic model given by Equation (3), showing R^2 values equal to 0.988 and 0.999, respectively. Reduced χ^2 values are equal to 16.774 and 0.196, respectively. All data corresponding to 2 and 5 mg L^{-1} are equal to the maximum adsorption efficiency, 100%, not represented in Figure 7. Additionally, comparison with pseudo-first order, pseudo-second order, Elovich and interparticle diffusion kinetic models [48] was performed through Bayesian information criterion and Akaike's information criterion computed in software Origin 2020, both concluding that Equation (3) is more likely to describe the adsorption kinetics.

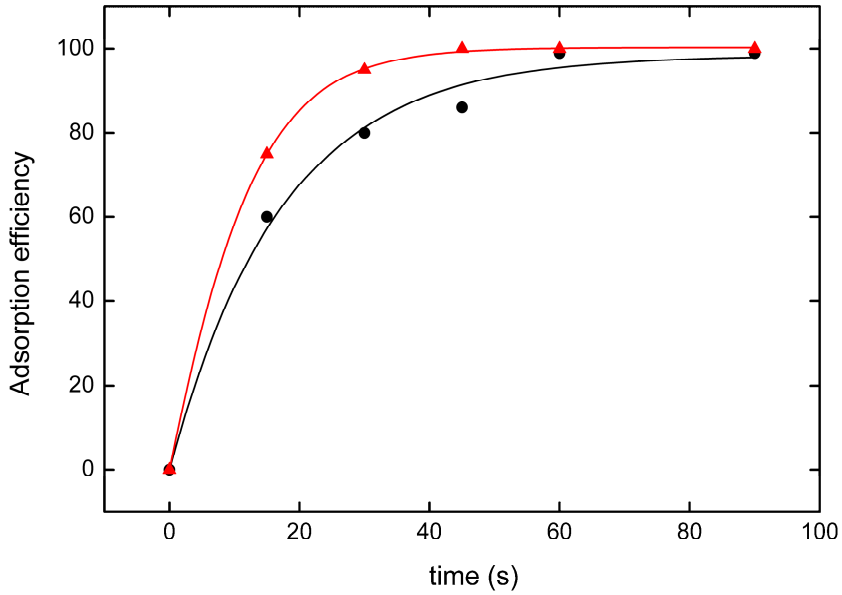

Figure 7. Dependence of the adsorption efficiency on time of contact between Fe_3O_4@AgNPs and nitrate for 50 mg L^{-1} of nitrate concentration and 500 µL of adsorbent (black dots), and 10 mg L^{-1} and 500 µL (red triangles). Solid lines are the fits to the kinetic model introduced by Equation (3).

3.5. Effect of Coexisting Anions on Nitrate Removal

The presence of anions such as sulphates, phosphates, carbonates and chlorides along with nitrates is common in waters samples [49,50]. The interference of these ions at different concentrations on nitrate adsorption was studied in this work, by adding them to the aquatic medium before the adsorption process was performed, determining the removal efficiency through spectrophotometry operating at 220 nm. Several scenarios of contaminated water were considered by varying the concentrations of these ions, based on methods from other works [31–33,51]. The molar ratio of nitrate/chloride and nitrate/phospate of 1:5 led to a slight decrease in the nitrate removal efficiency from 100.0% to 93.2% at 10 mg L^{-1} of nitrate concentration, 250 µL of Fe_3O_4@AgNPs suspension, at room temperature, pH 5 and 1 min of contact time. However, the molar ratio of nitrate/chloride and nitrate/phospate of 1:1 and 1:3 did not influence on nitrate adsorption. The presence of the other anions, sulphates and carbonates, was tested in the molar ratio P/anion from 1:1, 1:3 and 1:5, finding no significant influence on nitrate adsorption for the same experimental conditions. This fact shows that Fe_3O_4@Ag presents higher affinity towards anions with lower charge density.

3.6. Adsorption Isotherms

Adsorption isotherms characterize the relationship between the equilibrium values of the adsorption capacity, q_e (mg g^{-1}), and the adsorbate concentration, C_e (mg L^{-1}). Langmuir isotherm considers homogenous monolayer adsorption, described by the equation [33]:

$$\frac{1}{q_e} = \frac{1}{q_m} + \frac{1}{K_L q_m C_e} \tag{4}$$

where K_L is the Langmuir adsorption constant (L mg^{-1}) and q_m is the maximum adsorption capacity of the adsorbent (mg g^{-1}). This model adequately represents the fit to the experimental data for adsorption of nitrates to Fe_3O_4@AgNPs at pH = 5 and higher. In Figure 8 (left) the dependence of $1/q_e$ on $1/C_e$ at pH = 5 is shown. The fit to the Langmuir isotherm, Equation (4), gives rise to the best R^2 and reduced χ^2 values, equal to 0.998 and 1.886, respectively. A deeper study reveals that the shape of the isotherm curve is sensitive to the change of pH, and it has been previously reported by some authors that variations in

pH conditions can lead to different isotherm behaviors, described by different theoretical models [52]. Freundlich isotherm considers multilayer adsorption and, particularly, affinity between surface sites, which can be achieved when reducing pH due to the increase in positively charged surface sites [52]. Freundlich equation is [53]:

$$q_e = K_F C_e^{\frac{1}{n}} \quad (5)$$

where K_F and $1/n$ are known as the adsorption capacity and the adsorption intensity constants, respectively. Figure 8 (right) shows the dependence of $\log(q_e)$ on $\log(C_e)$ for adsorption of nitrates to Fe_3O_4@AgNPs at pH = 1. The nonlinear fit to Equation (5) gives rise to the best R^2 and reduced χ^2 values, equal to 0.99997 and 0.05092, respectively. By comparison, the data fit to Equation (4) shows $R^2 = 0.99982$ and $\chi^2 = 0.32504$, which reveals a better description for the equilibrium behavior at pH = 1 achieved by the Freundlich model. Other isotherms such as Temkin gave rise to worse fits.

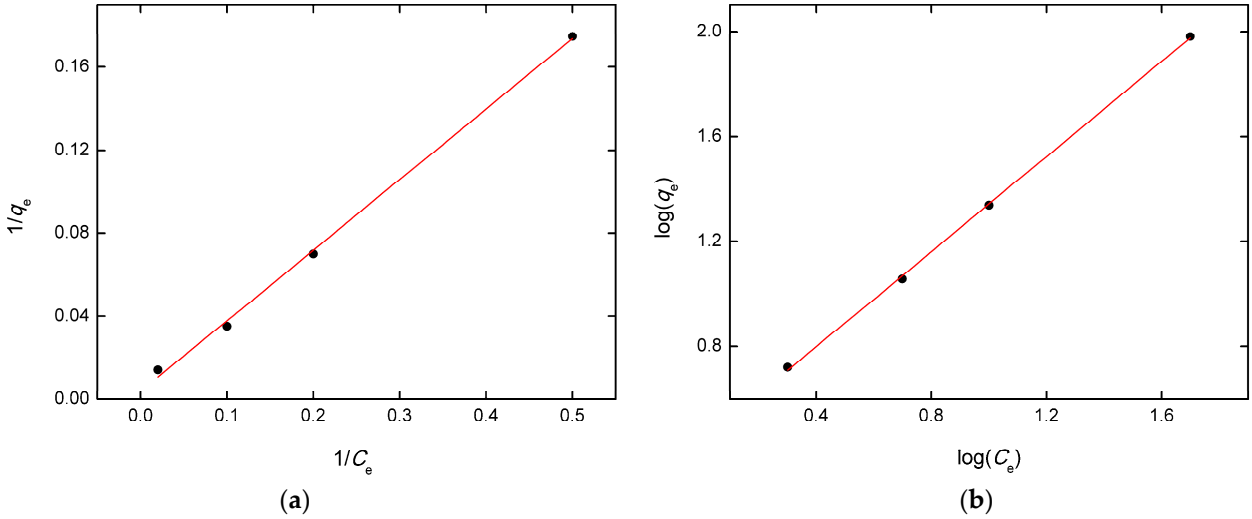

Figure 8. Langmuir (**a**) and Freundlich (**b**) isotherm plots for pH values equal to 5 and 1, respectively. Solid lines represent the fit to Equations (4) and (5), respectively. It is revealed that the decrease of pH enables the Freundlich isotherm as a better model for describing the equilibrium behavior of nitrate adsorption to Fe_3O_4@AgNPs.

3.7. Thermodynamic Analysis

The analysis of adsorption thermodynamics characterizes the nature of the process, i.e., physisorption or chemisorption, through the determination of the standard Gibbs free energy ΔG^0 (kJ mol^{-1}). Additionally, the estimation of the standard free enthalpy, ΔH^0 (kJ mol^{-1}), reveals if the process is exothermic or endothermic, while the standard entropy, ΔS^0 (kJ mol^{-1} K), gives information about the increase or decrease of order in the solid/liquid interface [33,54]. ΔG^0 values are determined from the equation:

$$\Delta G^0 = -RTln(K_D) \quad (6)$$

where R is the gas constant, T is the absolute temperature, and K_D is the so-called distribution coefficient:

$$K_D = \frac{q_e}{C_e} \quad (7)$$

Negative values for ΔG^0 are consistent with a spontaneous adsorption. Values in the range [−20, 0] kJ mol^{-1} reveal a physisorption process, while [−400, −80] kJ mol^{-1} correspond to chemisorption [33]. ΔG^0 interval was determined for the adsorption of nitrates to Fe_3O_4@AgNPs, for $C_e = 10$ mg L^{-1}, 250 µL of adsorbent and pH = 5, ranging temperature

from 278 to 343 K. The results show that ΔG^0 lies in the interval $[-15.75, -21.03]$ kJ mol^{-1}, which can be considered as a physicochemical adsorption process [55].

Van't Hoff equation relates variables T, ΔH^0, ΔS^0 and ΔG^0 (through Equation (6)) by the following expression:

$$\ln(K_D) = \frac{\Delta S^0}{R} - \frac{\Delta H^0}{RT} \quad (8)$$

In adsorption processes it is usual to find a unique linear dependence between $\ln(K_D)$ and $1/T$. For the adsorption of nitrates to Fe_3O_4@AgNPs described above, we distinguish three different behaviors. Figure 9 shows the plot $\ln(K_D)$ vs. $1/T$ for temperatures ranging from 278 to 343 K. Fitting Equation (8) to the low temperature region (right solid line) gives rise to $\Delta H^0 = 48.71$ kJ mol^{-1} and $\Delta S^0 = 0.23$ kJ mol^{-1} K, corresponding to an endothermic process with decrease in the order for the solid/liquid interface. The fit to the high temperature region (left straight line) shows $\Delta H^0 = -17.96$ kJ mol^{-1} and $\Delta S^0 = 0.0088$ kJ mol^{-1} K, indicative of an exothermic process with slight decrease in the order for the solid/liquid interface. The central T region shows no temperature dependence for $\ln(K_D)$.

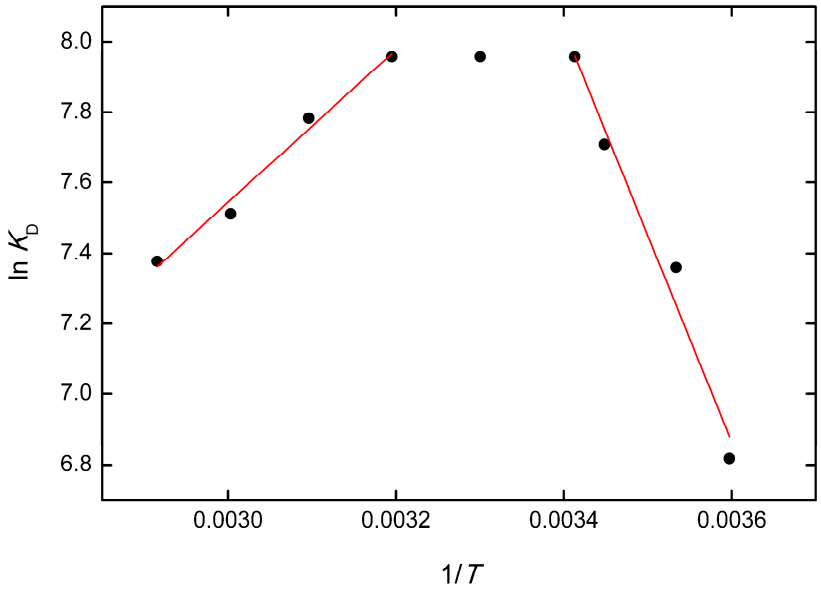

Figure 9. Van't Hoff plot $\ln(K_D)$ vs. $1/T$ for the adsorption of nitrates to Fe_3O_4@AgNPs at pH = 5, for $C_e = 10$ mg L^{-1} and 250 µL of adsorbent. The graph reveals a change from endothermic to exothermic process as T increases, separated by a central region showing no dependence on T. Solid lines are theoretical fits given by Equation (8).

3.8. Desorption and Recycling Nanoparticles

In order to reuse Fe_3O_4@AgNPs for successive adsorption processes, nanoparticles were separated from aqueous solution using a magnet, washed with a few milliliters of acetone and desorbed by employing 500 µL of NaOH solution 0.01 M. After that, NaOH solution was separated, and the nanoparticles were employed again to remove nitrate (10 mg L^{-1}) from aqueous solution under the experimental conditions describe before.

Fe_3O_4@AgNPs can be reused, remaining unchanged for two more cycles, and exhibiting 90% adsorption efficiency after the third regeneration and 81% after the fourth regeneration.

3.9. Adsorption of Nitrates onto Fe_3O_4@AgNPs in Real Seawater Samples

The method introduced in this work for the adsorption of nitrates from water solutions was tested in real seawater samples. Nitrates were analyzed for those samples and, afterwards, their adsorption was performed by using Fe_3O_4@AgNPs under the optimal experimental conditions described above. The results are summarized in Table 2.

Table 2. Adsorption of nitrate to Fe_3O_4@AgNPs in real seawater samples.

Sample	Absorbance before Adsorption	Absorbance after Adsorption	Removal Efficiency (%)
1	0.37	0.02	94.6
2	0.22	0.01	95.4
3	0.20	0.00	100

Removal efficiency values within the range 94.6–100% were achieved, slightly lower than those presented in the experimental procedure because seawater contains other anions at very high concentrations that could interfere in the adsorption process.

4. Conclusions

This work introduces a novel and simple method for the adsorption of nitrate from water samples using magnetic nanoparticles coated with nanomeric Ag. Different experimental conditions were studied showing to be optimal at pH = 5 and room temperature. 100% adsorption efficiency was reached in 60 s of contact time for nitrate concentration equal to 50 mg L^{-1}, employing 500 μL of Fe_3O_4@AgNPs. At lower nitrate concentrations, the contact time needed is just 15 s using 250, 100 and 100 μL of adsorbent for 10, 5 and 2 mg L^{-1} of nitrate concentration, respectively. Adsorption isotherms and thermodynamic studies reveal interesting behaviors in the removal process. Firstly, a strong pH-dependence for the adsorption equilibrium is found, characterized by Langmuir model at pH = 5 and Freundlich model at pH = 1. Secondly, thermodynamics reveals a transition from an endothermic to an exothermic physicochemical adsorption as temperature increases. The nanoparticles can be recycled by applying a few milliliters of a NaOH solution and they can be reused for two additional adsorption cycles, exhibiting no loss of the adsorption properties. In addition, the interference of other ions in the adsorption process was studied, showing that the presence in high concentrations of the species usually found in waters does not affect the adsorption, except for the extreme ratio nitrate/phosphate of 1:5. Moreover, the procedure was satisfactorily applied to real seawater samples, enabling the approach as a new and very efficient method for the decontamination of eutrophized waters.

Author Contributions: Conceptualization, Y.V.-M., M.C. and A.S.-M.; methodology, Y.V.-M., M.C., A.S.-M., M.Á.M.-P. and M.d.C.G.-O.; software, Y.V.-M., M.C. and A.S.-M.; validation, Y.V.-M., M.C., A.S.-M., M.Á.M.-P. and M.d.C.G.-O.; formal analysis, Y.V.-M., M.C., A.S.-M., M.Á.M.-P. and M.d.C.G.-O.; investigation, Y.V.-M., M.C., A.S.-M., M.Á.M.-P. and M.d.C.G.-O.; resources, Y.V.-M., M.C. and A.S.-M.; data curation, Y.V.-M., M.C., A.S.-M., M.Á.M.-P. and M.d.C.G.-O.; writing—original draft preparation, Y.V.-M., M.C. and A.S.-M.; writing—review and editing, Y.V.-M., M.C. and A.S.-M.; visualization, Y.V.-M., M.C., A.S.-M., M.Á.M.-P. and M.d.C.G.-O.; supervision, Y.V.-M., M.C. and A.S.-M.; project administration, Y.V.-M., M.C. and A.S.-M.; funding acquisition, Y.V.-M., M.C. and A.S.-M. All authors have read and agreed to the published version of the manuscript.

Funding: This research received no external funding.

Institutional Review Board Statement: Not applicable.

Informed Consent Statement: Not applicable.

Acknowledgments: The authors want to thank the University Centre of Defence at the Spanish Air Force Academy, for financial support.

Conflicts of Interest: The authors declare no conflict of interest.

References

1. Żołnierczyk, M.; Barbusiński, K. Physicochemical methods of nitrates removal from waste water. *Archit. Civ. Eng. Environ.* **2019**, *12*, 153–159. [CrossRef]
2. Payen, S.; Falconer, S.; Carlson, B.; Yang, W.; Ledgard, S. Eutrophication and climate change impacts of a case study of New Zealand beef to the European market. *Sci. Total Environ.* **2020**, *710*. [CrossRef] [PubMed]
3. Guo, C.; Chen, Y.; Xia, W.; Qu, X.; Yuan, H.; Xie, S.; Lin, L.S. Eutrophication and heavy metal pollution patterns in the water suppling lakes of China's south-to-north water diversion project. *Sci. Total Environ.* **2020**, *711*, 134543. [CrossRef]
4. Zhang, Y.; Liang, J.; Zeng, G.; Tang, W.; Lu, Y.; Luo, Y.; Xing, W.; Tang, N.; Ye, S.; Li, X.; et al. How climate change and eutrophication interact with microplastic pollution and sediment resuspension in shallow lakes: A review. *Sci. Total Environ.* **2020**, *705*, 135979. [CrossRef]
5. Zhou, Y.; Wang, L.; Zhou, Y.; Mao, X. Eutrophication control strategies for highly anthropogenic influenced coastal waters. *Sci. Total Environ.* **2020**, *705*, 135760. [CrossRef]
6. Constantinou, C.L.; Costa, C.N.; Efstathiou, A.M. Catalytic removal of nitrates from waters. *Catal. Today* **2010**, *151*, 190–194. [CrossRef]
7. Theologides, C.P.; Savva, P.G.; Costa, C.N. Catalytic removal of nitrates from waters in a continuous flow process: The remarkable effect of liquid flow rate and gas feed composition. *Appl. Catal. B Environ.* **2011**, *102*, 54–61. [CrossRef]
8. Ruiz-Bevia, F.; Fernandez-Torres, M.J. Comments on "Use of Rh (III)-Heteropolymolybdate as Potential Catalysts for the Removal of Nitrates in Human Drinking Water: Synthesis, Characterisation and Catalytic Performance" by María A. Jaworski et al. (Water Air Soil Pollut (2018) 229: 309). *Water Air Soil Pollut.* **2019**, *230*, 1–3. [CrossRef]
9. Ruiz-Beviá, F.; Fernández-Torres, M.J. Effective catalytic removal of nitrates from drinking water: An unresolved problem? *J. Clean. Prod.* **2019**, *217*, 398–408. [CrossRef]
10. Lacasa, E.; Cañizares, P.; Sáez, C.; Fernández, F.J.; Rodrigo, M.A. Removal of nitrates from groundwater by electrocoagulation. *Chem. Eng. J.* **2011**, *171*, 1012–1017. [CrossRef]
11. Abdel-Aziz, M.H.; El-Ashtoukhy, E.S.Z.; Zoromba, M.S.; Bassyouni, M.; Sedahmed, G.H. Removal of nitrates from water by electrocoagulation using a cell with horizontally oriented Al serpentine tube anode. *J. Ind. Eng. Chem.* **2020**, *82*, 105–112. [CrossRef]
12. Acharya, S.; Sharma, S.K.; Chauhan, G.; Shree, D. Statistical Optimization of Electrocoagulation Process for Removal of Nitrates Using Response Surface Methodology. *Indian Chem. Eng.* **2018**, *60*, 269–284. [CrossRef]
13. Anderson, J.A. Metal-promoted titania photocatalysis for destruction of nitrates and organics from aqueous environments. *Philos. Trans. R. Soc. A Math. Phys. Eng. Sci.* **2018**, *376*. [CrossRef]
14. Baly, E.C.C.; Heilbron, I.M.; Hudson, D.P. CXXX.—Photocatalysis. Part II. The photosynthesis of nitrogen compounds from nitrates and carbon dioxide. *J. Chem. Soc. Trans.* **1922**, *121*, 1078–1088. [CrossRef]
15. Richard, Y.; Thebault, P. Biological removal of nitrates—Report on 7 years of operation and progress. *Water Supply* **1992**, *10*, 151–160.
16. Janda, V.; Rudovsky, J. Removal of nitrate from drinking water by biological denitrificationp. *ChemInform* **1993**, *87*, 179–186.
17. Wąsik, E.; Bohdziewicz, J.; Blaszczyk, M. Removal of nitrates from ground water by a hybrid process of biological denitrification and microfiltration membrane. *Process Biochem.* **2001**, *37*, 57–64. [CrossRef]
18. Marecik, R.; Dembczyński, R.; Juzwa, W.; Chrzanowski, Ł.; Cyplik, P. Removal of nitrates from processing wastewater by cryoconcentration combined with biological denitrification. *Desalin. Water Treat.* **2015**, *54*, 1903–1911. [CrossRef]
19. Ketcha, M.J.; Manga, N.H.; Daouda, K.; Tchoua, N.P. Kinetic and equilibrium studies of the adsorption of nitrates ions in aqueous solutions by activated carbons and zeolite. *Res. J. Chem. Environ.* **2007**, *11*, 47–51.
20. Chabani, M.; Amrane, A.; Bensmaili, A. Kinetics of nitrates adsorption on Amberlite IRA 400 resin. *Desalination* **2007**, *206*, 560–567. [CrossRef]
21. Chabani, M.; Amrane, A.; Bensmaili, A. Kinetic modelling of the adsorption of nitrates by ion exchange resin. *Chem. Eng. J.* **2006**, *125*, 111–117. [CrossRef]
22. Milmile, S.N.; Pande, J.V.; Karmakar, S.; Bansiwal, A.; Chakrabarti, T.; Biniwale, R.B. Equilibrium isotherm and kinetic modeling of the adsorption of nitrates by anion exchange Indion NSSR resin. *Desalination* **2011**, *276*, 38–44. [CrossRef]
23. Adamu, H.; Shand, M.; Taylor, R.S.F.; Manyar, H.G.; Anderson, J.A. Use of carbon-based composites to enhance performance of TiO2 for the simultaneous removal of nitrates and organics from aqueous environments. *Environ. Sci. Pollut. Res.* **2018**, *25*, 32001–32014. [CrossRef]
24. Ferrando, L.; Matamoros, V. Attenuation of nitrates, antibiotics and pesticides from groundwater using immobilised microalgae-based systems. *Sci. Total Environ.* **2020**, *703*. [CrossRef]
25. Valiyeva, G.G.; Bavasso, I.; Di Palma, L.; Hajiyeva, S.R.; Ramazanov, M.A.; Hajiyeva, F.V. Synthesis of fe/ni bimetallic nanoparticles and application to the catalytic removal of nitrates from water. *Nanomaterials* **2019**, *9*, 1130. [CrossRef] [PubMed]
26. Dharmagunawardhane, D.S.; De Silva, N.L.; Gunatilake, U.B.; Yan, C.F.; Bandara, J. Removal of groundwater nitrates by heterogeneous supramolecular complexes-like photocatalytic system based on in-situ generated and highly active Ti^{3+}/Ti^{2+} states in the reduced TiO_2. *Mol. Catal.* **2019**, *470*, 89–96. [CrossRef]

27. Galan, C.R.; Silva, M.F.; Mantovani, D.; Bergamasco, R.; Vieira, M.F. Green synthesis of copper oxide nanoparticles impregnated on activated carbon using Moringa oleifera leaves extract for the removal of nitrates from water. *Can. J. Chem. Eng.* **2018**, *96*, 2378–2386. [CrossRef]
28. García-Fernández, M.J.; Sancho-Querol, S.; Pastor-Blas, M.M.; Sepúlveda-Escribano, A. Surfactant-assisted synthesis of conducting polymers. Application to the removal of nitrates from water. *J. Colloid Interface Sci.* **2017**, *494*, 98–106. [CrossRef] [PubMed]
29. Chianese, A.; Di Palma, L.; Petrucci, E.; Stoller, M.; Muradova, G.G.; Gadjieva, S.R.; Di Palma, L.; Vilardi, G. Nitrates Removal by Bimetallic Nanoparticles in Water. *Chem. Eng. Trans.* **2016**, *47*, 205–210.
30. Vicente-Martínez, Y.; Caravaca, M.; Soto-Meca, A.; Solana-González, R. Magnetic core-modified silver nanoparticles for ibuprofen removal: An emerging pollutant in waters. *Sci. Rep.* **2020**, *10*, 18288. [CrossRef]
31. López-García, I.; Vicente-Martínez, Y.; Hernández-Córdoba, M. Determination of ultratraces of mercury species using separation with magnetic core-modified silver nanoparticles and electrothermal atomic absorption spectrometry. *J. Anal. At. Spectrom.* **2015**, *30*, 1980–1987. [CrossRef]
32. Vicente-Martínez, Y.; Caravaca, M.; Soto-Meca, A. Total removal of Hg (II) from wastewater using magnetic nanoparticles coated with nanometric Ag and functionalized with sodium 2-mercaptoethane sulfonate. *Environ. Chem. Lett.* **2020**, *18*, 975–981. [CrossRef]
33. Vicente-Martínez, Y.; Caravaca, M.; Soto-Meca, A.; De Francisco-Ortiz, O.; Gimeno, F. Graphene oxide and graphene oxide functionalized with silver nanoparticles as adsorbents of phosphates in waters. A comparative study. *Sci. Total Environ.* **2020**, *709*, 136111. [CrossRef] [PubMed]
34. Shen, X.; Wang, Q.; Chen, W.; Pang, Y. One-step synthesis of water-dispersible cysteine functionalized magnetic Fe_3O_4 nanoparticles for mercury(II) removal from aqueous solutions. *Appl. Surf. Sci.* **2014**, *317*, 1028–1034. [CrossRef]
35. Cohen, H.; Gedanken, A.; Zhong, Z. One-step synthesis and characterization of ultrastable and amorphous Fe_3O_4 colloids capped with cysteine molecules. *J. Phys. Chem. C* **2008**, *112*, 15429–15438. [CrossRef]
36. Zhang, Y.R.; Shen, S.L.; Wang, S.Q.; Huang, J.; Su, P.; Wang, Q.R.; Zhao, B.X. A dual function magnetic nanomaterial modified with lysine for removal of organic dyes from water solution. *Chem. Eng. J.* **2014**, *239*, 250–256. [CrossRef]
37. Trivedi, M.K.; Dahryn Trivedi, A.B. Spectroscopic Characterization of Disodium Hydrogen Orthophosphate and Sodium Nitrate after Biofield Treatment. *Chromatogr. Sep. Tech.* **2015**, *6*. [CrossRef]
38. Karthikeyan, P.; Banu, H.A.T.; Meenakshi, S. Synthesis and characterization of metal loaded chitosan-alginate biopolymeric hybrid beads for the efficient removal of phosphate and nitrate ions from aqueous solution. *Int. J. Biol. Macromol.* **2019**, *130*, 407–418. [CrossRef] [PubMed]
39. Battas, A.; El Gaidoumi, A.; Ksakas, A.; Kherbeche, A. Adsorption study for the removal of nitrate from water using local clay. *Sci. World J.* **2019**, *2019*. [CrossRef]
40. Azari, A.; Kalantary, R.R.; Ghanizadeh, G.; Kakavandi, B.; Farzadkia, M.; Ahmadi, E. Iron-silver oxide nanoadsorbent synthesized by co-precipitation process for fluoride removal from aqueous solution and its adsorption mechanism. *RSC Adv.* **2015**, *5*, 87377–87391. [CrossRef]
41. López-Ramón, V.; Moreno-Castilla, C.; Rivera-Utrilla, J.; Radovic, L.R. Ionic strength effects in aqueous phase adsorption of metal ions on activated carbons. *Carbon* **2003**, *41*, 2020–2022. [CrossRef]
42. Moreno-Castilla, C. Adsorption of organic molecules from aqueous solutions on carbon materials. *Carbon* **2004**, *42*, 83–94. [CrossRef]
43. Adar, R.M.; Safran, S.A.; Diamant, H.; Andelman, D. Screening length for finite-size ions in concentrated electrolytes. *Phys. Rev. E* **2019**, *100*, 042615. [CrossRef]
44. Barton, B.I.; Lique, C.; Lenn, Y.D. Water Mass Properties Derived From Satellite Observations in the Barents Sea. *J. Geophys. Res. Ocean.* **2020**, *125*, e2019JC015449. [CrossRef]
45. Rodriguez, J.A. The adsorption of nitrogen dioxide, nitrate and sulfate on Ag(110): A quantum-chemical study. *Surf. Sci.* **1990**, *230*, 335–349. [CrossRef]
46. Al-Wabel, M.; Elfaki, J.; Usman, A.; Hussain, Q.; Ok, Y.S. Performance of dry water- and porous carbon-based sorbents for carbon dioxide capture. *Environ. Res.* **2019**, *174*, 69–79. [CrossRef]
47. Islam, A.; Khan, M.R.; Mozumder, S.I. Adsorption equilibrium and adsorption kinetics: A unified approach. *Chem. Eng. Technol.* **2004**, *27*, 1095–1098. [CrossRef]
48. Jun, B.M.; Heo, J.; Park, C.M.; Yoon, Y. Comprehensive evaluation of the removal mechanism of carbamazepine and ibuprofen by metal organic framework. *Chemosphere* **2019**, *235*, 527–537. [CrossRef]
49. Su, Y.; Yang, W.; Sun, W.; Li, Q.; Shang, J.K. Synthesis of mesoporous cerium-zirconium binary oxide nanoadsorbents by a solvothermal process and their effective adsorption of phosphate from water. *Chem. Eng. J.* **2015**, *268*, 270–279. [CrossRef]
50. Das, J.; Patra, B.S.; Baliarsingh, N.; Parida, K.M. Adsorption of phosphate by layered double hydroxides in aqueous solutions. *Appl. Clay Sci.* **2006**, *32*, 252–260. [CrossRef]
51. López-García, I.; Vicente-Martínez, Y.; Hernández-Córdoba, M. Determination of very low amounts of free copper and nickel ions in beverages and water samples using cloud point extraction assisted by silver nanoparticles. *Anal. Methods* **2015**, *7*, 3786–3792. [CrossRef]

52. Jeppu, G.P.; Clement, T.P. A modified Langmuir-Freundlich isotherm model for simulating pH-dependent adsorption effects. *J. Contam. Hydrol.* **2012**, *129–130*, 46–53. [CrossRef] [PubMed]
53. Ayawei, N.; Ebelegi, A.N.; Wankasi, D. Modelling and Interpretation of Adsorption Isotherms. *J. Chem.* **2017**, *2017*, 3039817. [CrossRef]
54. Tran, H.N.; You, S.J.; Hosseini-Bandegharaei, A.; Chao, H.P. Mistakes and inconsistencies regarding adsorption of contaminants from aqueous solutions: A critical review. *Water Res.* **2017**, *120*, 88–116. [CrossRef] [PubMed]
55. Xia, M.; Chen, Z.; Li, Y.; Li, C.; Ahmad, N.M.; Cheema, W.A.; Zhu, S. Removal of Hg(ii) in aqueous solutions through physical and chemical adsorption principles. *RSC Adv.* **2019**, *9*, 20941–20953. [CrossRef]